ISSN 1819-7140, Russian Journal of Pacific Geology, 2015, Vol. 9, No. 4, pp. 274–286. © Pleiades Publishing, Ltd., 2015.
Original Russian Text © V.Yu. Fridovsky, G.N. Gamyanin, L.I. Polufuntikova, 2015, published in Tikhookeanskaya Geologiya, 2015, Vol. 34, No. 4, pp. 39–52.

Structures, Mineralogy, and Fluid Regime of Ore Formation in the Polygenetic Malo-Taryn Gold Field, Northeast Russia

V. Yu. Fridovsky[a, c], G. N. Gamyanin[a, b], and L. I. Polufuntikova[c]

[a] *Institute of Diamond and Precious Metal Geology, Siberian Branch, Russian Academy of Sciences, pr. Lenina 39, Yakutsk, 677980 Russia*

e-mail: 710933@list.ru

[b] *Institute of Geology of Ore Deposits, Petrography, Mineralogy, and Geochemistry, Russian Academy of Sciences, Staromonetnyi per. 35, Moscow, 119017 Russia*

e-mail: gagmen@mail.ru

[c] *Ammosov Northeastern Federal University, ul. Belinskogo 58, Yakutsk, 677000 Russia*

e-mail: plio07@list.ru

Received October 29, 2014

Abstract—Detailed structural study of ore zones and deformations in host rocks reveals the multistage tectonic evolution of the Malo-Taryn ore field. Gold–quartz mineralization is confined to the interstratal and longitudinal thrust faults, where vein–stringer bodies are systematically oriented relative to the structures of the thrust stage. Antimony mineralization is superposed on gold–quartz mineralization in the same structures, being associated with veins formed during the shear stage of deformations. It is determined that the types of mineralization were formed in the following sequence: gold–bismuth, low-sulfide gold–quartz, berthierite–antimonite, and silver–antimony. Data on mineral assemblages and typomorphic features of minerals are reported. The isotope composition of minerals, temperature conditions, and composition of ore-bearing fluids are studied. It is established that the same minerals ascribed to different types of mineralization sharply differ in typomorphic features, which is caused by the different composition and genesis of the hydrothermal fluids. The superposition of different types of mineralization on one another within repeatedly activated tectonic structures that were fluid-permeable for a long time is an important indication of large-scale deposits.

Keywords: structure, deformations, polygenetic mineralization, mineralogy, isotope composition, temperature conditions, fluid, northeastern Russia

DOI: 10.1134/S1819714015040028

INTRODUCTION

In recent years, vein–stringer and stringer–disseminated gold mineralization has become the main object of exploration and prospecting works in northeastern Russia [1, 8–10, 12, 17]. In the Yana–Kolyma gold belt, this type includes the Natalka, Pavlik, Drazhnoe, Bazovskoe, Malo-Taryn, and other deposits related to Late Jurassic–Early Cretaceous orogenic events and associated tectonic and plutonic–metamorphic processes, which are best expressed in large extended fault zones. The Upper Indigirka tectonic zone in the Taryn ore cluster contains not only hydrothermal–metamorphic low-sulfide gold–quartz mineralization, but also gold–bismuth, gold–antimony, and silver–antimony types. The gold–bismuth and low-sulfide gold–quartz types of mineralization are related to the collisional–accretionary processes, while the gold–antimony and silver–antimony mineralizations were produced in relation with post-accretionary processes, which caused the wide development of deformations of different age and polygenetic mineralization within the same ore-hosting structures. The Taryn ore cluster includes the Dora-Pil, Sana-Maltan, and Malo-Taryn ore fields. These ore fields contain different types of mineralization in different volumes. In particular, the hydrothermal–metamorphic quartz–chlorite–carbonate mineralization is the most widespread in all ore fields and beyond them. The Dora-Pil ore field is dominated by the low-sulfide gold–quartz and silver–antimony mineralization [18]. Low-sulfide gold–quartz, gold–antimony, and silver–antimony ores are established at the Sana–Maltan ore field [19, 21]. Mineralization of the most diverse composition and age is found at the Malo-Taryn ore field (MTOF). The gold–bismuth, low-sulfide gold–quartz, berthierite–antimony, and silver–antimony types are juxtaposed there in repeatedly activated faults [20]. The detailed analysis of the ore zones, deformation structures in the host rocks, and ore composition makes it possible to decipher the evo-

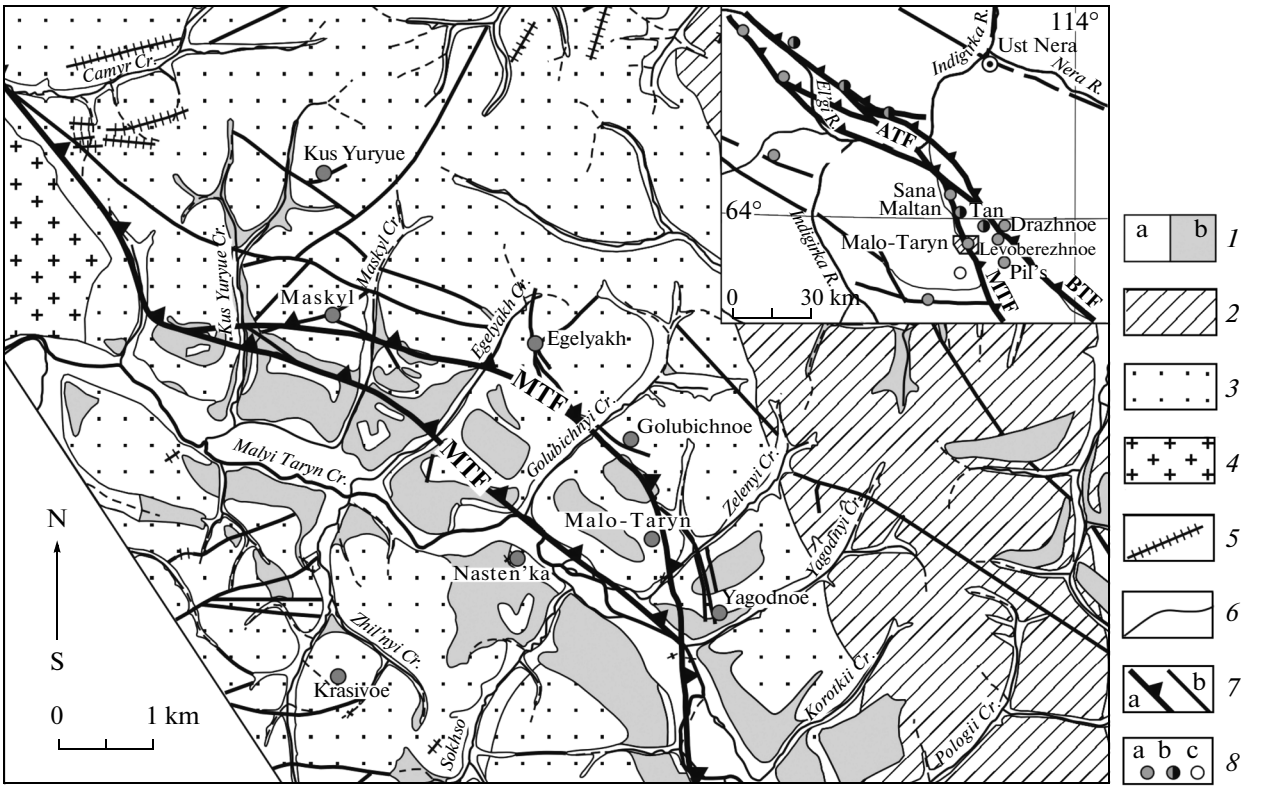

Fig. 1. Geological scheme of the Malo-Taryn ore field and adjacent territories using data from [1].
(*1*) Quaternary alluvial sediments: (a) Holocene, (b) Upper Pleistocene; (*2*) Lower Jurassic sediments J_1; (*3*) Upper Triassic sediments T_3; (*4*) Kurdat granitoid massif; (*5*) dikes of dioritic, andesitic, and basaltic porphyrites; (*6*) geological boundary; (*7*) faults: (a) Malo-Taryn, (b) others; (*8*) deposits and occurrences: (a) gold, (b) gold–antimony, (c) silver. Inset shows the position of the studied area. (ATF) Adycha–Taryn Fault, (MTF) Malo-Taryn Fault, (BTF) Bolshoi Taryn Fault.

lution of the tectonic structures and mineralization of the polygenetic MTOF.

The MTOF is located at the boundary of the hinterland zone of the Verkhoyansk fold-and-thrust belt and the Kular–Nera schist belt. The given geostructural position of the ore field caused repeated manifestation of tectonomagmatic activity and different-age ores, which are often superposed on one another in long-living tectonic zones. The MTOF is situated at the southwestern limb of the Malo-Taryn syncline and composed of the Triassic and Lower Jurassic trerrigenous sediments represented by siltstones, sandy siltstones, and less common mudstones and sandstones (Fig. 1). The spatial association of the Taryn ore cluster with granodiorite–granite massifs (Samyr and Kurdat) distinguishes it from other ore objects and offers an opportunity to study the relationships between mineralizations of different age, including that associated with magmatism. It was previously established that the formation of the productive gold mineralization of MTOF (130 ± 4 Ma) [1, 2] occurred after the emplacement of the Kurdat granitoid massif (141.2 Ma) [16], which cuts across Late Triassic terrigenous rocks. Sericite taken by us from quartz–chlorite–carbonate veinlets of the MTOF yielded an Ar–Ar age of 142.7 ± 1.4 Ma (A.V. Travin, Sobolev Institute of Geology and Mineralogy of the Siberian Branch, Russian Academy of Sciences). The veinlets are barren and may be ascribed to the early hydrothermal–metamorphic rocks scattered over the project area.

TECTONIC DEFORMATIONS AND OREBODY LOCALIZATION CONDITIONS

The main tectonic structure of the MTOF is the Malo-Taryn branch of the Adycha-Taryn fault. It is represented by a combination of faults and fracture zones of the predominant NW and more rarely WE and NS strike (Fig. 1). Northwest of the MTOF, the Adycha–Taryn fault defines the localization of the gold–quartz and gold–antimony mineralization of the Sana–Maltan ore field. The strike of the rocks on the limbs of the Malo-Taryn Fault (MTF) shows significant variations from NNW and NS in the northeastern limb to NW and NNE in the southwestern limb. In general, the rocks form a regional near-fault bend typical of sinistral displacements. Morphologically, the ore bodies of the MTOF represent mineralized brecciation zones (Zelenyi, Golubichnyi, and

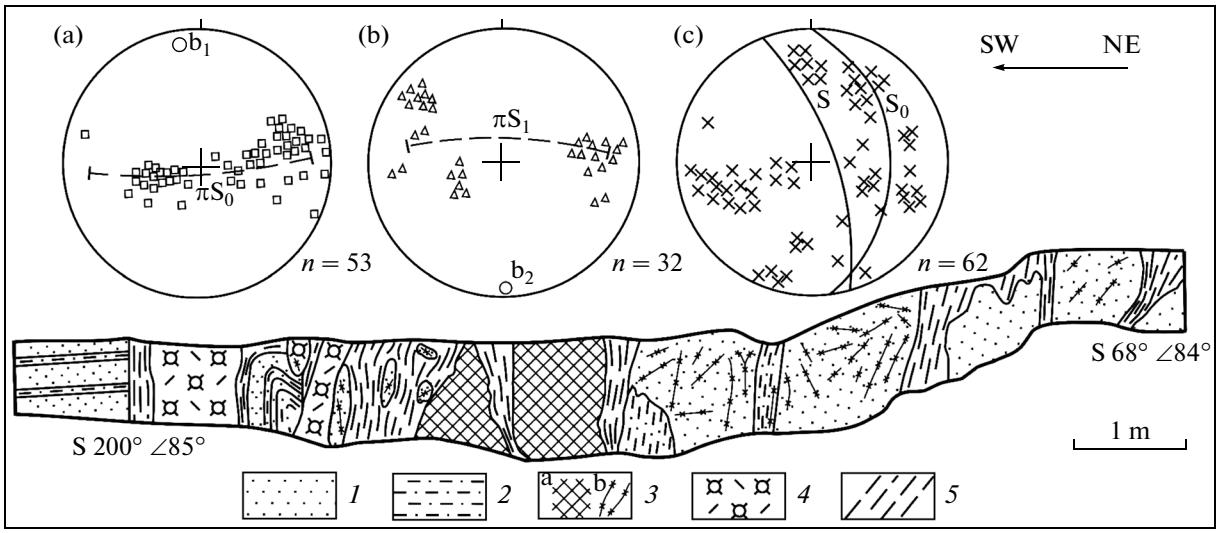

Fig. 2. Structure of the ore field, Zelenyi project area.
(*1*) sandstones; (*2*) siltstones; (*3*) quartz: (a) veins, (b) stringers; (4) dike of andesitic porphyrites; (*5*) mylonites. Pole diagrams for: (a) bedding S_0, (b) cleavage, and (c) quartz veins; S is the position of the fault. Hereinafter, points were plotted on the upper hemisphere.

Egelyakh project areas), as well as stockwork zones and lenticular bodies (Yagodnyi and Kus Yuryue project areas).

The best studied is the Zelenyi project area. It is located in the valley and watershed part of Zelenyi Creek, on the western limb of the Malo-Taryn syncline complicated by high order folds (Fig. 1). The host structures are zones of intense folding and brecciation with vein–stringer gold–quartz mineralization (Fig. 2).

The strike of this zone is conformable with the fold structures, varying from submeridional in the southern part of the area to northwestern (330°). Its structural forms were related to active interstratal motions that are synchronous with early reverse-thrust fault deformations of the Late Jurassic–Early Cretaceous stage in the evolution of the territory. The bedding plane S_0 shows dip-oriented sliding furrows, intrastratal ramps, and boudins of sandstones among siltstones. There are also symmetrical, asymmetrical, and recumbent folds F_1 with near-horizontal NNW-trending hinges. The bedding poles form a belt along the arc of the large circle, which is typical of cylindrical folds (Fig. 2a). The folds are associated with the fracture cleavage of the axial surface, which is the most intense in siltstones and attenuates in the coarse-grained rocks. In the fault zones, the cleavage is deformed into folds F_2 that are generally conformable to F_1 (Fig. 2b). The bedding presumably was subjected to the same deformations.

Statistical analysis of the attitude of the quartz veins and veinlets at the Zelenyi project area showed that their formation is tightly related to thrusting along the interstratal and longitudinal faults (Fig. 2c). For this reason, the veins and veinlets form systems aligned to these structural elements. One system of vein and veinlet, regardless of their strike, is perpendicular to the bedding So and ore-controlling fault S. The other system in general strikes in line with S_0 and S, but the veins and veinlets plunge at different angles to the east and west.

The ore zone is accompanied by subsidiary faults, one of which is traced along the bedrock of the Zelenyi Creek. The NE-trending fault was possibly formed during the accretionary–collisional stage in the evolution of the structure as a transverse ramp, and then was transformed into a fault plane with essentially vertical movements. The cleavage in the eastern limb of the transverse fault is turned to form folds with steep hinges, which reveal ptygmatite quartz–carbonate veins.

The Golubichnyi project area (The Golubichnyi Creek basin) is deformed by intense cleavage of submeridional strike, with steep SW- and E-dipping planes. This cleavage is usually cross-cutting, but is oriented conformably with bedding in the zones of coarse alternation of rocks. It frequently forms lenticular morphologies with microlithons up to 1–2 cm thick. The multistage dislocations are traced from cleavage deformations, sliding furrows, rock brecciation, and other structural features. The bedrocks of the creek expose a mineralized brecciation zone, the spatial position of which varies from conformable to cross-cutting the bedding at a small angle. It extends in the submeridional direction. This zone presumably represents a component of rear thrust running in the lower reaches of the Golubichnyi Creek. Hydrothermal rocks are represented by quartz–carbonate veins, veinlets, and stockwork-like zones confined mainly to sandstone beds. The poles of the quartz veins and vein-

lets on a stereographic projection are arranged mainly along the bedding.

In the bedrock of the Kus Yuryue Creek (eponymous project area), the contacts of sandstones and siltstones are activated by interstratal thrusts of western and southwestern vergence. Thick faults have not been recovered in the natural attitude; however, their presence may be inferred from the wide development of tectonites. The strike of the rocks varies from northwestern to submeridional (dip azimuth of 50°–90°, angle of 46°–61°), in line with the structures of the regional bend of the rocks. Several vein systems of different ages are developed in the upper reaches of the Kus-Yuryue Creek. The early veins are interstratal with characteristic banded structure and represent hydrothermal–metamorphic quartz—chlorite–carbonate mineralization. Two systems of synchronous quartz–carbonate veins of the productive stage are distributed in the intercalated sandstones and siltstones, at some angle to their attitude. The first system dips to the west and northwest, while the latter dips to the south at moderately steep angles. Both systems are perpendicular to lamination.

Thus, the structural analysis of the spatial position of the gold–quartz veins and veinlets has revealed their tight link with interstratal and oblique thrusts and rock attitude. The gold–quartz veins form systems that are aligned to the thrust structures. For this reason, the spatial position of the veins of the same system in the different parts of the ore field may differ, but their relationships with the ore-controlling deformation structures are preserved.

Deformations superposed on the gold–quartz mineralization were studied in the middle reaches of Egelyakh Creek (eponymous area). The rocks show near-meridional strike and steep eastern azimuths of dip (85°–70°). The creek runs along the rock strike for a significant distance, and a narrow canyon with nearly vertical walls is formed in the areas coinciding with the faults (Fig. 3).

Intense repeated tectonic deformations and sliding furrows of different direction are observed over the entire extent of the Egelyakh area. The fault zone up to 0.5 m thick and consisting of silicified mylonites is mapped in the right bank of the creek. It lies subconformably with the footwall rocks. The rocks of the hanging limb are deformed into open fold F_4 with hinges steeply dipping northeast (dip azimuth of 25° at angle of ∠60°) (Fig. 3b). Shear deformations are usually developed within narrow zones on the limbs of longitudinal faults. It should also be noted that the rocks 1.0–1.5 m east of the fault zone change their strike to NW orientation, which is conformable to the Adycha–Taryn Fault. Taking into account this fact, we may conclude that the regional bend of the rocks known in the MTOF is of the chevron type and also related to the later regional shearing, which is widely expressed by horizontal sliding furrows on the bedding planes, especially in the rocks of different competence.

Examination of the fracture structures in the Egelyakh area revealed six fracture systems. The first system is parallel to the bedding, near-meridional fault, and dips in the same direction (Fig. 3d). The second system dips gently to the east. The third system is perpendicular to the bedding and dips steeply to the south. The NW-trending fracture systems cutting the fault zone sometimes displace the bedding. These systems are ascribed to one paragenesis and their formation is related to fold and thrust dislocations. The calculated position of the paleotectonic stress axes is as follows: σ_3 76°, ∠20°; σ_1 305°, ∠71°; σ_2 170°, ∠14° (Fig. 3e). The late sinistral deformations are associated with the development of NE-trending fracture system S: σ_3 122° ∠3°; σ_1 205°, ∠31°; σ_2 28°, ∠68° (Fig. 4f). It is important to draw attention to the fact that the orientations of the measured and calculated sliding furrows coincide (Figs. 3d, 3f).

MINERAL COMPOSITION OF THE ORES

Mineralogical data indicate that the MTOF contains several types of mineralization: (1) gold–bismuth; (2) main economic low-sulfide gold–quartz; (3) berthierite–antimony; and (4) epithermal silver–antimony.

The gold–bismuth mineralization is represented by thin (2–4 cm) branching suvbertical stringers in sandstones. They have been found to contain quartz–muscovite–pyrrhotite–Co–Ni sulfoarsenide (Table 1, an. 1–6) and bismuth–sulfotelluride (Table 1, an. 12–16) assemblages. The composition of the nickel, cobalt, and iron sulfoarsenides are listed in Table 1 (an. 1–3, 5–6). It was established that Co and Ni are practically absent in the arsenopyrite, whereas their contents in the loellingite, danaite, and gersdorffite reach up to 10%, which is typical of minerals from weakly eroded deposits of such types [6]. Based on atomic absorption data, the minerals of this assemblage frequently contain 50–150 ppm gold. Bismuth minerals (Table 1, an. 12–16) are represented by bismuthinite and minerals of homological series: tetradymite, joseite A and B, and tellurobismutite [4].

The bismuth minerals are distinguished by the presence of Se and significant (up to 2.5%) admixture of Pb (Table 1, an. 12–15), which are typical of minerals from the gold deposits of the Adycha–Taryn metallogenic zone. They are associated with native fine (0.01–0.1 mm) gold with fineness varying in a wide range of 750–960 ‰.

The described gold–bismuth mineralization has much in common with the mineralization of the known Ergelyakh gold–bismuth deposit, the age of which was determined from wall-rock sericte as 114–125 Ma [7].

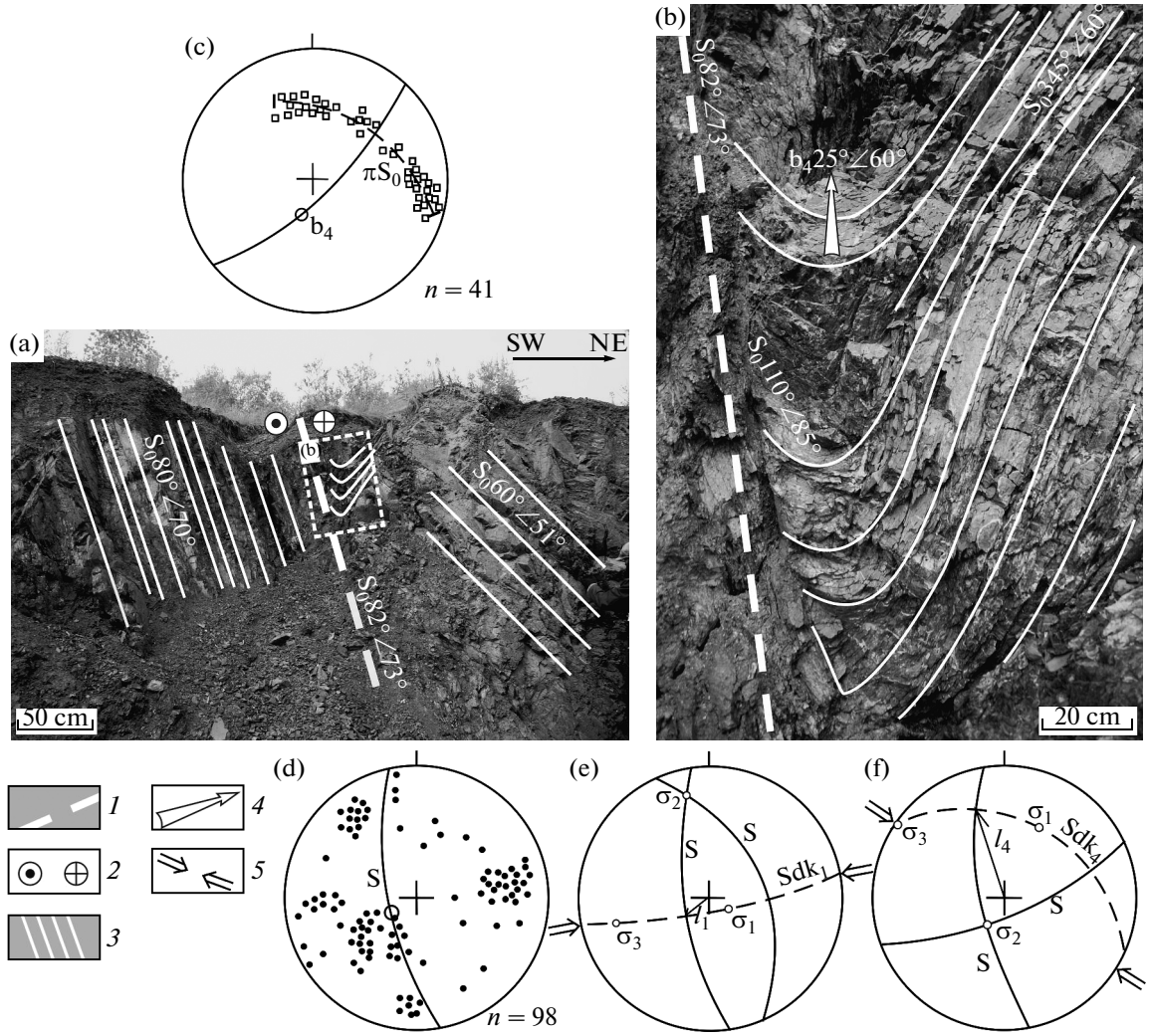

Fig. 3. Deformations of rocks in the submeridional fault zone, middle reaches of Egelyakh Creek.
(*1*) fault S; (*2*) sinistral strike-slip fault; (*3*) bedding S_0; (*4*) hinge of fold b_4; (*5*) compression direction. (a) strike and dip of rocks on limbs of near-meridional fault; (b) near-fault fold F_4; (c) bedding pole πS_0 of fold F_4 (dashed line) and position of axial surface (solid line), b_4 hinge of fold F_4; (d) poles of fractures on the limbs of submeridional fault, open circle is axis of roughness; (e, f) reconstruction of stress fields: (σ_3) is compression axis; (σ_1) extension axis; (σ_2) intermediate axis; (Sdk_1) dynamokinematic plane; first stage of deformations D_1; (Sdk_4) dynamokinematic plane; fourth stage of deformations D_4; (l_1, l_4) calculated direction of rock displacement of the first and fourth stages of deformations, respectively (S) position of conjugate chips.

The gold–quartz low-sulfide mineralization is represented by morphologically intricate quartz veins (10–40 cm thick and 50–100 m long) and stringers (1–0 cm thick and up to 1 m long) with sharp swells and pinches.

The ore bodies have a sufficiently uniform mineral composition: quartz 85–95%, carbonate (ankerite) 5–15%, and ore minerals around 1–2%. Several mineral assemblages are distinguished, which sequentially replace each other without signs of intersection, corrosion, and replacement.

The pyrite–arsenopyrite–quartz metasomatic assemblage around the simple veins composes near-selvage zones of wall-rock metasomatites up to 50 cm wide. The SiO_2 content reaches 90% within a 1–5 cm zone near the selvages and decreases to 75% at a distance of 40 cm. The metasomatic zones contain uneven dissemination of cubic pyrite metacrystals and fine-prismatic arsenopyrite.

In the metasomatites, pyrite ubiquitously prevails over arsenopyrite. The former may reach 10–20%, whereas arsenopyrite accounts for no less than 3%. Arsenopyrite is usually confined to the near-selvage (2–5 cm) zones of the metasomatites. Arsenic metapyrite from MTOF is either absent or occurs in subordinate amounts (0.2–0.7%). The metasomatic arsenopyrite of MTOF is ascribed to the low-sulfur variety (Table 1, an. 7), which is typical of most low-sulfide gold–quartz deposits of the Adycha–Taryn metallogenic zone [4]. The metapyrite contains

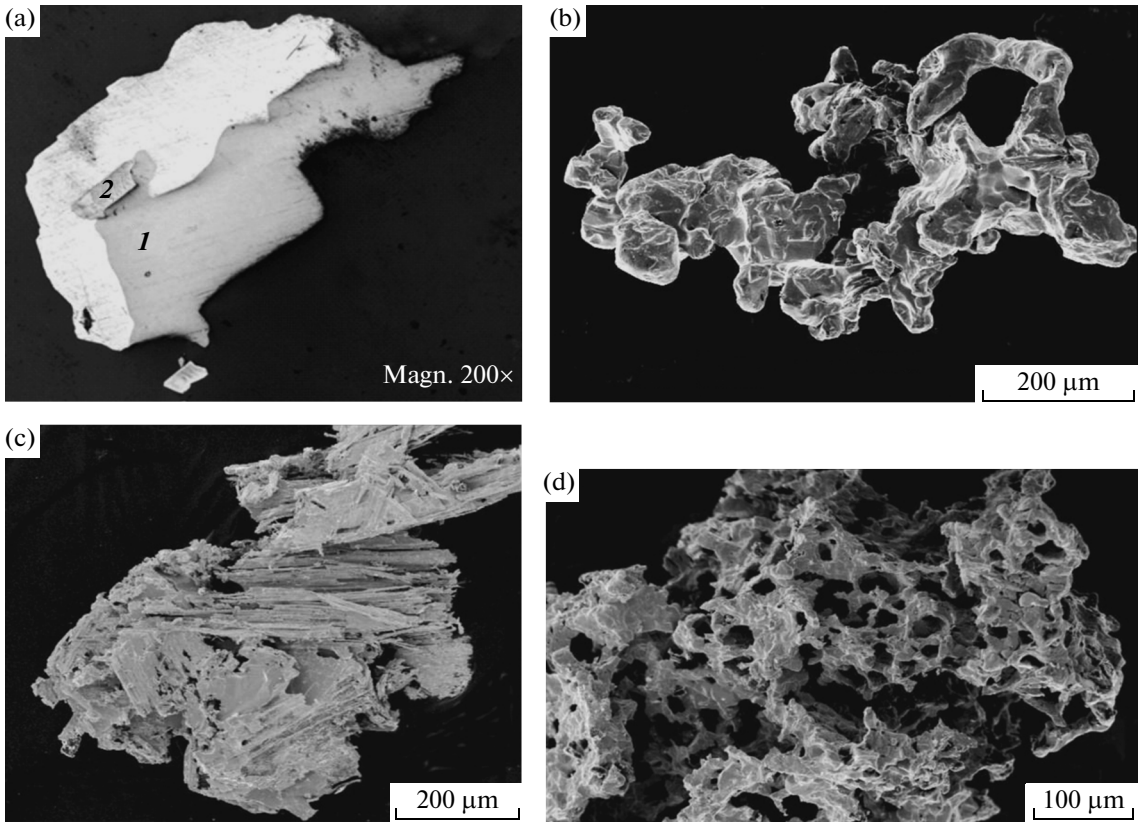

Fig. 4. Gold microstructures.

(a) intergrowths of gold with galena (*1*) and arsenopyrite inclusion in gold (*2*); (b–d) morphology of gold grains from associations with different minerals: (b) intergrown with galena, (d) intergrown with sulfosalts, (d) in quartz. Associated minerals are dissolved in HNO_3 or HF. Scanning, JEOL JSM-6480LV. Analyst N.V. Leskova

7–12 ppm Au (Table 2), 1–16 ppm Ag, 80–270 ppm Co, and 30–720 ppm Cu. The arsenopyrite contains 6–8 ppm Au (Table 2). The variations of the Ag content are within the same ranges as the Au content. Pb and Zn in small amounts (up to 100 ppm) also occur in the metasomatic sulfides. The Sb content is somewhat higher (up to 1000 ppm), reaching up to 1% in the arsenopyrite from the antimonite–berthierite ores.

The matrix of the ore bodies is made up of pyrite–arsenopyrite–quartz stringer assemblage. The typomorphic features of the quartz are two thermoluminescence peaks, moderate crystallinity degree (50–60%), low Li_2O (5–12 ppm), and unit cell volume of 112.990–112.998 $Å^3$. The pyrite and arsenopyrite were formed simultaneously with the quartz and are observed in it as pockets (up to 2–3 cm) and dispersed small euhedral (up to 5 mm) or shapeless grains. The relations between the pyrite and arsenopyrite indicate their simultaneous precipitation. The arsenopyrite more frequently than the pyrite is spatially associated with native gold, which often cuts it along the microcracks. The pyrite has a nonstoichiometric composition, with a clear predominance of Fe, which indicates an S deficit in the ore forming fluid (Table 1, an. 11). It contains admixture of As (often more than 0.5 wt %), as well as hundredths of a percent of Co, Ni, and Bi. According to microprobe analysis, the arsenopyrite is characterized by the slight predominance of S over As and low concentrations (<0.2 wt %) of trace Co, Ni, Sb, and, sometimes, Sn, Ge, and V. Such features of arsenopyrite composition are typical of the deposits of the base-metal subtype of low-sulfide quartz–gold formation [6]. It was found that the arsenopyrite contains Co, Ni, and Sb (<0.2 wt %). Gold–chalcopyrite–sphalerite–galena assemblage sporadically occurs. It consists mainly of galena (60–70%) and sphalerite (25–30%). The sulfides of this association most frequently occur as small disseminated rare grains confined to pyrite and arsenopyrite accumulations. The gold-rich zones practically always contain single sulfide grains of this assemblage. Sphalerite is the most widespread mineral. Its composition is listed in Table 1 (an. 17). Its dark brown to black color is caused by the steady Fe content within 8–10%. It contains emulsion dissemination of single chalcopyrite grains. The sphalerite contains up to 0.3% Cd. Spectral analysis revealed the permanent presence of 0.3–0.9% Sn and 0.02–0.4% In, which is not typical of the gold deposits of the Adycha–Taryn zone. Galena has a practically stoichiometric composition (Table 1, an. 18). It most frequently occurs in intergrowths with gold (Fig. 4a).

Table 1. Composition of ore minerals of the Malo-Taryn ore field

Ordinal no.	Mineral	Fe	As	Co	Ni	Sb	Bi	Ag	Pb	Zn	Cu	Te	Se	S	Total
1	Gersdorffite[1]	15.98	62.62	8.05	6.41	–	–	–	–	–	–	–	–	6.67	99.72
2	Ni-danaite[1]	19.27	58.42	6.84	5.31	–	–	–	–	–	–	–	–	9.85	99.69
3	Co–Ni-lollingite[1]	20.28	71.06	4.31	3.67	–	–	–	–	–	–	–	–	0.59	99.91
4	Pyrrhotite[3]	59.50	0.00	0.06	0.15	–	–	–	–	–	–	–	–	40.18	99.89
5	Arsenopyrite[1]	33.70	46.32	0.10	0.00	–	–	–	–	–	–	–	–	19.07	99.18
6	Arsenopyrite[1]	34.26	44.56	0.02	0.01	0.13	–	–	–	–	–	–	–	20.26	99.24
7	Arsenopyrite[2]	34.11	45.67	0.03	0.05	0.11	–	–	–	–	–	–	–	19.54	99.51
8	Arsenopyrite[3]	33.87	44.76	0.04	0.05	0	–	–	–	–	–	–	–	21.12	99.84
9	Arsenopyrite[5]	33.96	43.14	–	–	2.34	–	–	–	–	–	–	–	19.77	99.21
10	Pyrite[2]	46.55	0.56	0.05	0.05	0.07	–	–	–	–	–	–	–	53.87	101.15
11	Pyrite[3]	47.19	0.15	0.04	0.03	0.18	–	–	–	–	–	–	–	51.36	98.95
12	Bismutite[1]	–	–	–	–	0.27	79.88	0	0.63	–	–	0.34	0.29	18.32	99.73
13	Tetradymite[1]	–	–	–	–	0.2	63.24	0	2.43	–	–	27.51	0.59	5.64	99.50
14	Joseite A[1]	–	–	–	–	0.24	77.17	0	1.54	–	–	12.84	0.44	8.00	99.68
15	Joseite B[1]	–	–	–	–	0.24	71.94	0	0.89	–	–	22.51	0.43	4.22	99.47
16	Tellurobismuthinite[1]	–	–	–	–	0.25	74.24	0	2.34	–	–	22.49	–	–	99.43
17	Sphalerite[3]	8.50	–	–	–	–	–	–	–	58.34	0.19	–	–	33.66	100.68
18	Galena[3]	0	–	–	–	–	–	0.23	86.63	–	–	–	–	12.59	99.45
19	Tetrahedrite[3]	3.39	–	–	–	29.54	–	–	–	4.55	36.12	–	–	25.07	98.67
20	Freibergite[5]	5.62	–	–	–	27.07	–	15.87	–	2.21	25.04	–	–	22.98	98.79
21	Meneghinite[3]	–	–	–	–	21.36	–	–	60.67	–	–	–	–	17.59	99.62
22	Boulangerite[3]	–	–	–	–	25.07	–	–	55.24	–	–	–	–	17.59	99.62
23	Berthierite[4]	12.94	–	–	–	56.94	–	–	0.13	–	–	–	–	29.08	99.09
24	Antimonite[4]	0	–	–	–	72.01	–	–	-	–	–	–	–	27.93	98.94

(1) From gold–bismuth veins; (2–3) from gold-bearing metasomatites (2) and veins (3); (4) from berthierite–antimonite veins; (5) from cryptogranular quartz veins. Dash denotes element is absent. Analyses were performed on a JEOL JSM-6480LV microprobe at the Institute of Diamond and Precious Metal Geology, Siberian Branch, Russian Academy of Sciences. Analyst N.V. Leskova. Contents in wt %.

Table 2. Results of atomic absorption analysis of sulfides from ore bodies of the Malo-Taryn ore field

Ordinal no.	Mineral	Ag	Au	Cu	Co
1	Pyrite*	5.4; 7.2; 8.1	6.3; 8.9; 10.1	283; 337; 387	124; 138; 151
2	Pyrite**	7.5; 8.3; 12.6	117; 137; 154	41; 48; 62	82; 99; 117
3	Pyrite***	49; 76	480; 605	274; 353	62; 77
4	Arsenopyrite*	5; 9	5.7; 10.2	43; 57	78; 90
5	Arsenopyrite**	16.3; 21; 32	195; 251; 364	44; 60; 75	114; 129; 154

* From metasomatites; ** from gold-bearing veins; *** from cryptogranular quartz. Analysis was performed at the Institute of Diamond and Noble Metals Geology of the Siberian Branch of the Russian Academy of Sciences. Analyst A.N. Sannikova. Contents, in ppm.

Gold in a quartz matrix is observed in intergrowths with arsenopyrite, galena, and boulangerite. It outlines pyrite and arsenopyrite grains or penetrates into these minerals along microcracks. Gold with sphalerite, and more frequently galena, forms intergrowths of cocrystallizing minerals with even boundaries and sometimes even intergrowths of their crystals. In the acicular aggregates of sulfoantimonites, gold is localized along their elongated grains.

Gold occurs in diverse morphologies. Bladed, openwork–dendritic, and clotty–dendritic morphologies are typical of gold particles intergrown with pyrite and arsenopyrite. Gold penetrates into their cataclased aggregates to cement them. The gold is dominated by massive forms (including crystals) in association with late sulfides and occurs as elongated lamellar and dendritic aggregates with sulfoantimonites. The most diverse morphologies of gold are observed in quartz (Fig. 4). The fineness of the gold depends on the associated mineral. Gold in association with galena is characterized by the lowest fineness (894–910‰), which sequentially increases in association with arsenopyrite (901–925‰) and sulfoantimonite (930–960‰), reaching its highest values in association with antimonite (980–995‰).

The main mineral of the *sulfosalt–carbonate assemblage* is carbonate, variable amounts of which occur ubiquitously. In composition, it corresponds to the ankerite–dolomite group with variable FeO/MgO (0.6–2.3). The contents of the oxides vary within following ranges: MgO 9.5–18.4; FeO 13.5–22.5; MnO 0.02–1.3; and SrO 0–0.35. Sulfosalts also occur sporadically; they were precipitated slightly earlier than the carbonates and form inclusions in the latter. Sulfosalts are represented by tetrahedrite, meneghinite, and boulangerite (Table 1, an. 19–22). Tetrahedrite occurs exclusively as fine grains in association with acicular sulfoantimonites or separately in quartz cavities. In composition, it is typical tetrahedrite with very low Ag <0.3% (Table 1, an. 19). Meneghinite and boulangerite were found together, sometimes in association with tetrahedrite and gold. Their compositions are close to the theoretical ones (Table 1, an. 21, 22). The carbonate from this assemblage is the latest mineral and is localized in cavities among the quartz. In the brecciated quartz, it acts as a cementing or cross-cutting material.

The berthierite–antimonite mineralization occurs sporadically. The compositions of berthierite and antimonite are stoichiometric (Table 1, an. 23, 24). Quartz veins and stringers with antimonite and berthierite, often containing pyrite, are grouped into northwestern systems of the stockwork type. The thickness of the stringers varies from 0.1 to 2–3 cm and the thickness of the veins reaches 70–80 cm. Small stringers contain mainly berthierite, while the large stringers and veins contain antimonite. The superposition of this mineralization on the products of the gold stage is often accompanied by intense corrosion of the early milky-white quartz and sulfides of the veins and metasomatites. Sericite (composition, in wt %, average of four analyses: SiO_2 43.49, TiO_2 0.22, Al_2O_3 35.36, FeO 0.58, MgO 0.94, Na_2O 0.13, and K_2O 7.63. Total 95.51) from the beresites is replaced by ripidolite (composition in wt %, average of three analyses: SiO_2 25.36, Al_2O_3 28.76, FeO 12.19, MgO 12.04. Total 88.66). The chlorite localized among the stringers of columnar quartz with berthierite pockets has the same composition. Berthierite also forms very fine injections in these metasomatites. The antimonite-rich zones contain relicts of early gold–quartz ores. Small-scale reprecipitation of quartz results in the formation of its regenerated transparent crystals. The regenerated quartz has elevated content of Li_2O (0.021%). It is also characterized by a large unit cell volume (113.084 $Å^3$) and low crystallinity degree (43%). The neomorphous arsenopyrite and pyrite have elevated Sb contents (up to 0.3%). The early gold in these cases has a cavernous surface and brownish tint, being similar to "mustard" spongy gold from gold–antimony deposits [5]. Newly formed redeposited gold usually forms very small crystals intergrown with antimonite. They have high fineness 975–987‰. The composition of the berthierite and antimonite (Table 1) is close to the stoichiometric proportions of the components.

The silver–antimony mineralization has a wide areal distribution not only in the Malo-Taryn ore field, but also over the entire Adycha–Taryn fault zone, although rich mineralization occurs only in the submeridional zones of the Taryn subvolcano. This late

Table 3. Sulfur isotope composition of sulfides and carbon and oxygen isotope compositions of carbonates from different types of mineralization of the Malo-Taryn ore field

	$\delta^{34}S$ CDT	^{13}C pD_B	^{18}O smw
Hydrothermal–metamorphic			
Pyrite	9.1; 9.5		
Carbonate		–1.1	20.3
Gold–bismuth			
Arsenopyrite	–2.8; –3.7		
Carbonate		–6.9; –5.86	5.7; 2.1
Gold–quartz			
Arsenopyrite	–1.44; –0.96–1.14; –0.86; –2.13; –1.56		
Pyrite	–1.83; –2.82; –1.23; –1.15; –1.1		
Carbonate		–8.1; –7.5; –7.7	16.1; 16.4; 18.7
Berthierite–antimonite			
Berthierite	–0.6; –1.3		
Antimonite	–0.75; –0.55		
Carbonate		–10.5; –10.4; –11.2; –12.1	15.0; 15.3; 15.8; 15.8
Silver–antimony			
Pyrite	0.23; 0.34		
Carbonate		–11.57; –11.3	2.3; 4.7

Analysis was performed at the isotope-geochemical laboratory of the Institute of Geology of Ore Deposits, Petrography, Mineralogy, and Geochemistry, Russian Academy of Sciences. Analyst E.O. Dubinina.

epithermal mineralization is represented by stringers and veins of spherulitic, cryptogranular, or collomorphic–nodular quartz with poor sulfide dissemination. It was revealed at all deposits of the Taryn ore field [18, 19, 21]. However, the scales of its manifestation are different. Veins of dark gray to black cryptogranular quartz cross cutting and cementing the products of low-sulfide gold–quartz mineralization are observed at the Malo-Taryn Deposit. This quartz in its typomorphic features (Li_2O 300–500 ppm, unit cell volume V_{uc} 113.21 Å^3, crystallinity degree CD, 34–41%) is similar to the quartz from the silver–antimony deposits developed among the Taryn subvolcano. The cryptogranular quartz from the sulfides contains mainly dissemination (sometimes intense) of fine-grained to dust-like pyrite with scarce grains of rhombohedral arsenopyrite. The pyrite always contains As (up to 0.7%) and rarely Co and Ni (Table 1, an. 10, 11). Atomic absorption analysis of this pyrite revealed elevated (Table 2) concentrations of Au (599 ppm) and Ag (66 ppm). The arsenopyrite from the cryptogranular quartz veins has elevated Sb concentrations (1.6–2.3 wt %, Table 1, an. 9), which is a typomorphic feature of the silver–antimony mineralization of the Verkhoyansk–Kolyma Mesozoides [4]. Fahlore is freibergite (Table 1, an. 20).

ISOTOPE COMPOSITION OF MINERALS, TEMPERATURE CONDITIONS AND COMPOSITION OF ORE-GENERATING FLUID

The isotope compositions of the minerals from different types of mineralization in the Malo-Taryn ore field were analyzed in order to determine the sources of the components of the ore-forming fluid. Table 3 presents the results of measurement of $\delta^{34}S$ in the pyrite, arsenopyrite, berthierite, and antimonite. Isotope data on the minerals from the hydrothermal–metamorphic mineralization, the mineralogy of which was previously studied by the authors [18, 19, 21], are shown for comparison. It was established that the pyrite from the hydrothermal–metamorphic veins has the heaviest sulfur isotope composition (Table 3), which may indicate a significant contribution of sulfur from the host rocks. The pyrite from the gold–quartz mineralization is characterized by $\delta^{34}S$ from –1.1 to –2.82‰. The pyrite from the silver–antimony mineralization (Table 3) is characterized by a near-zero, relatively heavy sulfur isotope composition.

The arsenopyrite from the gold–bismuth mineralization is characterized by light sulfur isotope composition (–2.8, –3.7‰), while the sulfur in the arsenopyrite from the gold–quartz deposits has a heavier isotope composition: from –0.86 to –2.13‰. The close sulfur isotope compositions of the pyrite and arsenopyrite indicate that no sulfur isotopic fraction-

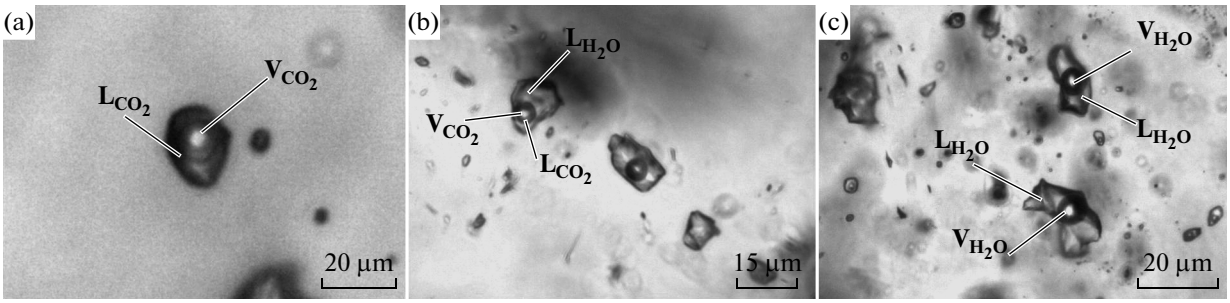

Fig. 5. Types of fluid inclusions in quartz from ore veins.
(a) Primary CO_2-rich inclusion (type 1); (b) primary CO_2–H_2O inclusion with liquid CO_2 (type 2); (c) secondary low-temperature two-phase fluid inclusion (type 3). (L_{H_2O}) aqueous solution, (V_{H_2O}) gas, (L_{CO_2}) liquid CO_2, (V_{CO_2}) gaseous CO_2.

ation occurred during their crystallization. The values of $\delta^{34}S$ for the berthierite and antimonite are close to zero values. Crystallization of the minerals from a single ore-forming fluid is accompanied by natural fractionation of the sulfur isotope composition toward its lighter compositions, which is not observed for berthierite and antimonite, the latest minerals. This may indicate a different nature of the fluid that precipitated these minerals. In general, the sulfur isotope composition shows a clear increase in the series gold–bismuth → gold–quartz → berthierite–antimonite → silver–antimony mineralization. Thus, the values of $\delta^{34}S$ of the sulfides for each hydrothermal type of mineralization have specific features which indicate the source and peculiarity of the fluids that precipitated these minerals. In general, the obtained sulfur isotope compositions indicate a magmatic source of ore-generating fluid.

The values of $\delta^{13}C$ and $\delta^{18}O$ for the carbonates from different types of mineralization of the Malo-Taryn Deposit are shown in Table 3. The carbonates from the metamorphic–hydrothermal and silver–antimony types of mineralization are represented by calcite and the other types by carbonates of the ankerite–dolomite series. The presented data indicate that the carbonates of the hydrothermal–metamorphic type sharply differ from the other carbonates in the lightest $\delta^{13}C$ and very heavy $\delta^{18}O$ (Table 3). The carbonates of the silver–antimony mineralization show an opposite pattern (Table 3): light carbon isotope composition and slightly heavy oxygen isotope composition. The carbonate from the gold–bismuth mineralization (Table 3) is characterized by moderately light and, correspondingly, heavy carbon and oxygen isotope compositions. At the same time, the carbonates of the gold–quartz and berthierite–antimonite types are sufficiently close in isotope composition: average $\delta^{13}C$ (–7.7 and –11.1‰) and $\delta^{18}O$ (17.2 and 15.5‰), respectively, with the heavier carbon and oxygen isotope compositions in the gold–quartz mineralization. In general, the oxygen and carbon isotope compositions of the carbonates decrease from the gold–quartz and berthierite–antimonite types to the gold–bisumth and further to the silver–antimony types. The presented data indicate the significant role of metamorphic waters during the formation of hydrothermal–metamorphic carbonates and the partial contribution of these waters during the formation of the gold–quartz and berthierite–antimonite mineralization.

Microthermometric studies of aqueous fluid were carried out on a Linkam THMSG-600 microscope heating stage (analyst V.Yu. Prokof'ev, Institute of Geology of Ore Deposits, Petrography, Mineralogy, and Geochemistry, Russian Academy of Sciences) within the temperature range from –196 to 600°C. The salt composition of the solutions, salt concentrations, and pressure were determined using known techniques [3, 11, 15, 23]. Aqueous extract from the inclusions was analyzed by different methods in the 0.5-g sample (fraction of 0.5–0.25 mm) at the Central Institute of Geological Exploration for Base and Precious Metals (analyst Yu.V. Vasyuta) using the technique published in [13].

Thermobarometric studies of the fluid inclusions were carried out only for quartz from the low-sulfide gold–quartz mineralization (analyst V.Yu. Prokof'ev, Institute of Geology of Ore Deposits, Petrography, Mineralogy, and Geochemistry, Russian Academy of Sciences), because the fluid inclusions in the quartz from the silver–antimony veins were too small for studies and it was impossible to extract a pure quartz sample from the berthierite–antimonite ores. The quartz from the ore veins of the MTOF contains two types of primary and primary–secondary fluid inclusions: CO_2-rich (type 1) and CO_2–H_2O (type 2) inclusions, which are syngenetic and indicate a heterogeneous state of the ore-forming fluid. In addition, it was found that the quartz from MTOF contains numerous secondary two-phase (type 3) fluid inclusions (Fig. 5). Most of the fluid inclusions are 1–20 μm in size and have negative crystal or irregular morphology.

Based on thermo- and cryometric studies of individual fluid inclusions, the ore-forming fluids of MTOF were entrapped within a temperature range of

Table 4. Major and trace element composition of the ore-forming fluid from different types of mineralization of the Malo-Taryn ore field

Components	Gold–quartz		Berthierite–antimonite		Silver–antimony	Gold–bismuth
	with arsenopyrite*	with galena and sphalerite*	with berthierite*	with antimonite*		
Major components, g/kg H_2O						
SiO_2	0.0	0.0	0.0	0.0	0.0	505
CO_2	154.3	49.2	277.8	555.4	11.9	964
CH_4	22.2	6.1	32.9	21.0	0.5	555
Cl	7.7	2.3	12.8	4.4	0.0	40.4
SO_4	0.0	0.0	0.0	5.4	17.3	–
HCO_3	38.1	17.6	306.7	134.4	281.4	114
Na	11.6	5.5	20.3	8.2	15.9	619
K	0.7	0.0	1.6	0.5	25.2	72
Ca	5.6	2.1	34.6	15.2	3.3	14
Mg	0.4	0.2	32.7	15.7	41.8	1.9
Trace elements, mg/kg H_2O						
As	7408	91	296	232	432	1732
B	1035	459	1843	986	3063	40837
Li	86	38	67	124	9800	785
Rb	0	0	4	0	215	4
Sr	69	32	1237	430	1648	722
Sb	26	9	348	176	412	7
Mn	0	0	560	447	0	16
Cu	8	27	5	16	127	377
Zn	52	101	115	39	47	523
Pb	67	16	0	10	94	6
Ba	0	3	12	3	2120	14
W	0	1	9	4	0	0
Au	0	1	0	0	0	0
Fe	0	0	948	1082	11727	545
Ni	47	1	11	20	28	40
V	1	0	4	1	66	0
Cr	3	0	10	12	26	42
Se	0	0	0	0	5	1697

Analyses were performed at the Analytical Laboratory of the Central Research Institute of Geological Exploration for Base and Precious Metals using techniques of [3, 11, 15, 23]. Analyst Yu.V. Vasyuta. * Association of quartz with minerals.

318–253°C at pressure of 760 bar and contained dissolved sodium and magnesium carbonates (concentration of 5.9–2.6 wt % NaCl equiv.) and CO_2 (6.6–3.4 mol/kg solution) and methane (1.0–0.6 mol/kg solution). The primary inclusions show negative crystal shape and are represented by two–phase and syngenetic monophase gas vacuoles, which contain liquid CO_2 with admixture of 6–11 mol % CH_4. The secondary fluid inclusions contained aqueous solution with salinity of 6.5–2.2 wt % NaCl equiv. and were homogenized into a liquid phase at 230–169°C. Note the high density of the fluid (0.80–1.02 g/cm^3) and homogenization of the gas inclusion into a liquid phase.

Data on the major and trace element composition of the gas–liquid inclusions are presented in Table 4. It is seen that the maximum concentrations of the fluid components were found in the silver–antimony and berthierite–antimonite types of mineralization, while the lowest contents in the low-sulfide gold–quartz type with base metal mineral assemblage. It was estab-

lished that the ore-forming fluid in each type of mineralization is characterized by a peculiar composition:

the gold–bismuth type (Au–Bi) is characterized by sodium bicarbonate siliceous composition with gas phase consisting of 60% CO_2 and 40% CH_4;

the low-sulfide gold–quartz type (Au–Q) is characterized by calcium–sodium–bicarbonate fluid with 80% CO_2 in the gas component;

the antimony type (Sb) has a calcium–magnesium–bicarbonate composition with gas phase consisting mainly of CO_2;

the silver–antimony type (Ag–Sb) is characterized by potassium–magnesium–sulfate–bicarbonate composition.

The fluids from different types of mineralization sharply differ in trace element composition and concentrations. In general, the elements for each type of mineralization may be arranged in a series in order of their decreasing abundance in solution (concentration, mg/kg H_2O: >1000 shown in bold; 100–1000 shown in bold italics; 10–100 in italics; and <10 in normal font):

Au–Bi type: **B**, **As**, **Se**, ***Li***, ***Sr***, ***Fe***, ***Zn***, ***Cu***, *Cr*, *Ni*, *Mn*, *Ba*, *Sb*, Pb, and Rb;

Au–Q type: **As**, **B**, *Zn*, *Li*, *Sr*, *Pb*, *Sb*, *Ni*, Cu, Ba, Cr, W, Au, and V;

Bt–Ant type: **B**, **Fe**, **Sr**, ***Mn***, ***Sb***, ***As***, *Li*, *Zn*, *Ni*, *Cu*, Ba, Cr, W, Pb, V, and Rb;

Ag–Sb type: **Fe**, **Li**, **B**, **Ba**, **Sr**, ***As***, ***Sb***, ***Rb***, ***Cu***, *Pb*, *V*, *Zn*, *Ni*, *Cr*, and Se.

These concentration series indicate primarily that the high contents of specific elements in the aqueous extract are not correlated with the mineral composition of ores and cannot be explained by "contamination," but rather are defined by the source of the components. We suggest that the most probable explanation in this case is the entrapment of lithophile and some ore components (Fe, As) by ore-forming fluids of these types of mineralization during their migration through the host rocks to the discharge sites.

CONCLUSIONS

MTOF shows an increase in the intensity of fold-and-thrust deformations, reaching maximum values in the zone of the long-evolving ore-controlling fault and its branches. The gold–quartz mineralization is localized in the interstratal and longitudinal thrust faults; the vein–stringer bodies form systems that are aligned to the structures of the thrust stage. In the same structures, this mineralization is overprinted by another association, which is associated with shear deformation. This stage caused activation of faults, tectonic reworking of previously formed structures, their complication, and the development of near-fault NE-trending faults that overprinted early NW-trending folds. Similar folds accompanying the formation of gold–antimony mineralization are established in the Central zone of the Maltan Deposit [21] and at the Malyutka Deposit of the Dora-Pil ore field [18].

The material presented above reveals the multistage and polygenetic nature of MTOF mineralization, which is represented by several types: early gold–bismuth and low-sulfide gold–quartz types are cut by the late berthierite–antimonite and silver–antimony types. Geological observations indicate that they have different age, which is confirmed by the intersection, brecciation, and cementation of ores of early types of mineralization by younger types with clear signs of corrosion, regrouping, and redeposition of matter.

The same minerals from different types of mineralization differ in their typomorphic features: chemical composition, content of trace elements, sulfur isotope composition of sulfides, and carbon and oxygen isotope compositions of carbonates. The compositions of the fluid inclusions in quartz from different types of mineralization clearly indicate that the ore-forming fluids that formed the different types of mineralization are different and independent.

The above-mentioned facts indicate that the MTOF structures were penetrated by fluids from different depth levels over a long period, which led to the superposition of the post-acrretionary mineralization of the Late Cretaceous–Early Cenozoic Taryn metallogenic zone on the accretionary mineralization of the Adycha–Nera metallogenic zone. The juxtaposition of different types of mineralization within the same, repeatedly activated tectonic structures is an important indication of large deposits [4, 14, 22].

ACKNOWLEDGMENTS

This study was supported by the Russian Foundation for Basic Research (project no. 14-17-00465), and by the base budget project of the Institute of Diamond and Noble Metal Geology of the Siberian Branch of the Russian Academy of Sciences (project no. VIII.72.2.5).

REFERENCES

1. G. Yu. Akimov, A. V. Kryuchkov, T. L. Krylova, and A. A. Sidorov, "The Taryn vein–disseminated ore deposit: a new type of gold mineralization in the Verkhnyaya Indigirka Region, Yakutia," Dokl. Earth Sci. **397A** (6), 737–742 (2004).
2. G. Yu. Akimov, "New age data on gold–quartz mineralization in the Verkhnyaya Indigirka area, Yakutia," Dokl. Earth Sci. **398**, 895–898 (2004).
3. A. S. Borisenko, "Cryometric study of salt composition of gas–liquid inclusions in minerals," Geol. Geofiz., No. 8, 16–27 (1977).
4. A. V. Volkov, "The distribution and formation conditions of gold deposits in tectono-magmatic activization zones of the northeast of Russia," Geol. Ore Dep. **47** (3), 181–187 (2005).

5. G. N. Gamyanin, Yu. Ya. Zhdanov, I. Ya. Nekrasov, and N. V. Leskova, ""Mustard" gold from gold–stibium ores of East Yakutia," Nov. Dannye Mineral., No. 34, 13–20 (1987).
6. G. N. Gamyanin, *Mineralogical–Genetic Aspects of Gold Mineralization of the Verkhoyansk–Kolyma Mesozoides* (GEOS, Moscow, 2001) [in Russian].
7. G. N. Gamyanin, N. A. Goryachev, A. G. Bakharev, P. P. Kolisnichenko, A. I. Zaitsev, E. N. Diman, and N. V. Berdnikov, *Conditions of Initiation and Evolution of the Gold–Magmatic Systems in the Mesozoides of Northeast Asia* (MPO SVNTs DVO RAN, Magadan, 2003) [in Russian].
8. N. A. Goryachev, O. V. Vikent'eva, N. S. Bortnikov, V. Yu. Prokof'ev, V. A. Alpatov, and V. V. Golub, "The world-class Natalka gold deposit, Northeast Russia: REE patterns, fluid inclusions, stable oxygen isotopes, and formation conditions of ore," Geol. Ore Dep. **50** (5), 363–390 (2008).
9. V. I. Goncharov, S. V. Voroshin, and V. A. Sidorov, *Natalka Gold Deposit* (SVKNII DVO RAN, Magadan, 2002) [in Russian].
10. *Gold Deposits of Russia (*Akvarel', Moscow, 2010) [in Russian].
11. V. A. Kalyuzhnyi, *Principles of the Theory of Mineral-Forming Fluids* (Nauk. dumka, Kiev, 1982) [in Russian].
12. M. M. Konstantinov, E. M. Nekrasov, A. A. Sidorov, and S. F. Struzhkov, *Gold Giants of Russia and World* (Nauch. mir, Moscow, 2000) [in Russian].
13. S. G. Kryazhev, Yu. V. Vasyuta, and M. K. Kharrasov, "Method of bulk analysis of inclusions in quartz," in *Proceedings of 11th International Conference on Thermobarogeochemistry, Aleksandrov, Russia, 2003* (VNII-SIMS, Aleksandrov, 2003), pp. 6–10.
14. V. M. Kuznetsov, N. A. Goryachev, S. V. Zhigalov, and N. E. Savva, "Structure and ore potential of the Mayakit–Khurchan ore placer cluster," Vestn. SVNTs DVO RAN, No. 4, 37–51 (2011).
15. E. Roedder, *Fluid Inclusions*, Rev. Mineral. (Mineral. Soc. Am., Washington, 1984), Vol. 12.
16. *Tectonics, Geodynamics, and Metallogeny of the Sakha Republic (Yakutia)* (MAIK "Nauka/Interperiodika", Moscow, 2001) [in Russian].
17. V. Yu. Fridovsky, "Analysis of deformation structures of the El'ga ore cluster, East Yakutia," Otechestvennaya Geol., No. 4, 39–45 (2010).
18. V. Yu. Fridovsky, G. N. Gamyanin, and L. I. Polufuntikova, "Dora-Pil ore field: structure, mineralogy, and geochemistry of ore formation medium," Rudy Met., No. 5, 7–21 (2012).
19. V. Yu. Fridovsky, G. N. Gamyanin, and L. I. Polufuntikova, "Sana gold–quartz deposit, Taryn ore cluster," Razved. Okhr. Nedr, No. 12, 3–7 (2013).
20. V. Yu. Fridovsky and G. N. Gamyanin, "Long-evolving fault zone of the Taryn ore cluster and settings of mineralization localization," in *Proceedings of the All-Russian Scientific-Practical Conference on Geology and Mineral-Raw Resources of Northeast Asia, Yakutsk, Russia, 2013* (SVFU, 2013), Vol. 2, 246–252 [in Russian].
21. V. Yu. Fridovsky, G. N. Gamyanin, and L. I. Polufuntikova, "Gold–quartz and antimony mineralization in the Maltan deposit in Northeast Russia," Russ. J. Pac. Geol. **8** (4), 276–287 (2014).
22. V. G. Khomich, I. I. Fatyanov, and N. G. Boriskina, "Metallogenic analysis of the type gold-bearing districts in the southern and eastern framing of the North Asian Craton: geotectonic position, geological structure, and specifics of formation," Russ. J. Pac. Geol. **7** (6), 52–63 (2013).
23. P. L. P. Collins, "Gas hydrates in CO_2-bearing fluid inclusions and the use of freezing data for estimation of salinity," Econ. Geol. **74**, 1435–1444 (1979).

Recommended for publishing by N.A. Goryachev

Translated by M. Bogina